Experimental Measurement of the Hilbert-Schmidt Distance between Two-Qubit States as a Means for Reducing the Complexity of Machine Learning

Vojtěch Trávníček,[1,*] Karol Bartkiewicz,[1,2,†] Antonín Černoch,[3,‡] and Karel Lemr[1,§]
[1]RCPTM, Joint Laboratory of Optics of Palacký University and Institute of Physics of Czech Academy of Sciences, 17. listopadu 12, 771 46 Olomouc, Czech Republic
[2]Faculty of Physics, Adam Mickiewicz University, PL-61-614 Poznań, Poland
[3]Institute of Physics of the Czech Academy of Sciences, Joint Laboratory of Optics of PU and IP AS CR, 17. listopadu 50A, 772 07 Olomouc, Czech Republic

(Received 3 July 2019; published 23 December 2019)

We report on the experimental measurement of the Hilbert-Schmidt distance between two two-qubit states by many-particle interference. We demonstrate that our three-step method for measuring distances in the Hilbert space is far less complex than reconstructing density matrices and that it can be applied in quantum-enhanced machine learning to reduce the complexity of calculating Euclidean distances between multidimensional points, which can be especially interesting for near term quantum technologies and quantum artificial intelligence research. Our results are also a novel example of applying mixed states in quantum information processing. Usually working with mixed states is undesired, but here it gives the possibility of encoding extra information as the degree of coherence between the given two dimensions of the density matrix.

DOI: 10.1103/PhysRevLett.123.260501

Introduction.—Quantum information protocols such as teleportation [1,2] and cryptography [3–5] established in the field of quantum information processing [6,7] have a significant impact on modern communications [8–10]. In fact, early quantum communications networks based on quantum teleportation have already been reported [11–14] and experimentally realized [15,16]. Their physically guaranteed security [17] and potential for scalability makes them a preferable choice for future communications networks. In quantum communications the quality of a transmission channel is crucial. It is due to security reasons, where imperfections of the communication channel lead to signal degradation known as noise. This noise can be subsequently exploited by potential eavesdroppers [18,19]. Therefore, tools for the diagnostics of the transmission channels are in demand. In quantum communications theory one can quantify the accuracy of a signal transmission by measuring the distance in the Hilbert space between the transmitted and received states. The most prominent distance measures include the Uhlmann-Jozsa fidelity (Bures metrics), trace distance, and the Hilbert-Schmidt distance (HSD) (for overviews, see, e.g., [20–22]).

These distance measures are also essential for a field of quantum machine learning. Where a common method for classification algorithms (e.g., k means) is to perform a distance measurement among M sample vectors of dimension N. This procedure is a core subroutine for other machine learning algorithms, e.g., supervised and unsupervised nearest-neighbor algorithms. Quantum machine learning emerges as a new field of research in quantum information processing with linear optics, where the benefits of applying this platform are unaffected by unavoidably nondeterministic implementation of a universal set of gates [23]. It has been already demonstrated that by using quantum resources one can reduce the complexity of the algorithm from $\mathcal{O}[\mathrm{poly}(MN)]$ to $\mathcal{O}[\log(MN)]$ [23–25]. Here, we demonstrate that by measuring the distance in terms of HSD we obtain the complexity of the distance-measuring algorithm to $\mathcal{O}(\log N)$ by using a different approach from that in Ref. [24]. The HSD is defined as

$$D_{\mathrm{HS}}(\hat{\rho}_1,\hat{\rho}_2) \equiv \sqrt{\mathrm{Tr}[(\hat{\rho}_1-\hat{\rho}_2)^2]}, \tag{1}$$

where $\hat{\rho}_1$ and $\hat{\rho}_2$ are the density matrices representing the two quantum, in general mixed, states. The HSD is a Riemannian metrics, which makes it appropriate for applying in machine learning problems. Moreover, in contrast to trace distance, HSD is nonincreasing under decoherence [20,21]. For simplicity, let us explain how to implement the k-means algorithm for finding two clusters of 3D points enclosed in a cube using qubits. A density matrix for a qubit can be expressed via Pauli matrices $\hat{\sigma}_i$ and the identity matrix $\hat{I}$ as $\hat{\rho} = \frac{1}{2}\hat{I} + u_1\hat{\sigma}_x + u_2\hat{\sigma}_y + u_3\hat{\sigma}_z$. Let us use this kind of matrix to encode a data point $\vec{u} = (u_1, u_2, u_3)$ for $|\vec{u}| \leq \frac{1}{2}$ and $i = 1, 2, 3$. The task is to assign different N-dimensional data points (here $N = 3$) to k clusters (let us set *two* clusters) with sample reference vectors $\vec{v}_1$ and $\vec{v}_2$. A data point $\vec{u}$ is classified to the closest cluster. It turns out

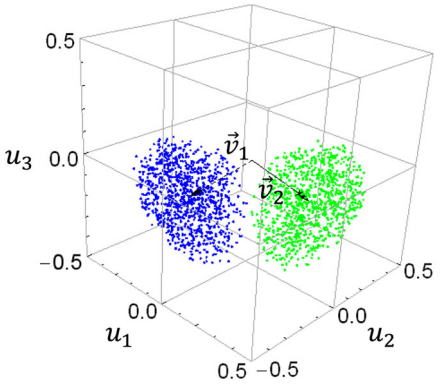

FIG. 1. An example of two clusters of 1000 3D points assigned to the nearest center of a cluster (given by arrows $\vec{v}_1$ or $\vec{v}_1$). By encoding vectors $\vec{u}$ and $\vec{v}_i$ for $i = 1, 2$ as density matrices of qubits and by measuring distances between them as HSD we properly assign all the points to one of the clusters. Thus, for two-qubit states we can classify 15-dimensional points. Note that all the points are embedded in a Bloch ball of a radius of $\frac{1}{2}$.

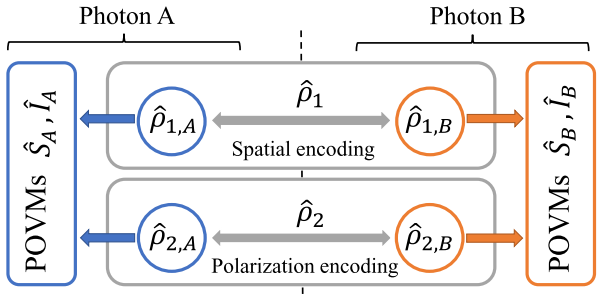

FIG. 2. Conceptual scheme for measuring the Hilbert-Schmidt distance between two-qubit states. In general, two different states $\hat{\rho}_1$ and $\hat{\rho}_2$ are encoded into polarization and spatial modes of photon A and B, respectively. Photons A and B are then simultaneously measured by POVMs $\hat{I}$ and $\hat{S}$, where the 2 degrees of freedom are addressed holistically at the same time. The operators $\hat{I}$ and $\hat{S}$ are the identity and singlet state projection where $\hat{S} = |\Psi^-\rangle\langle\Psi^-|$.

that by a proper choice of mapping between vectors and density matrices, we can ensure that Euclidean distance $|\vec{v}_{1,2} - \vec{u}|$ and HSD are equal up to a constant factor. Thus, by assigning data points to a cluster corresponding to the nearest reference vector, depending on the distribution of $\vec{u}$, we can end up with two clearly separable clusters as shown in Fig. 1. In the next step of the k-means algorithm, new positions of centers of clusters are found as mean positions of points belonging to a given cluster. The classification process is repeated. If points do not change their assigned clusters, the algorithm is terminated. Note that the same applies to larger systems, e.g., for a 15-dimensional (in Hilbet-Schmidt space) physically accessible Bloch ball (or the inscribed hypercube if the components of $\vec{u}$ need to represent data from a segment $[-l, l]$, where l is the size of the hypercube) the corresponding state is given as $\hat{\rho} = \frac{1}{4}\hat{I} \otimes \hat{I} + \sum_{i=1,2,3}(u_i\hat{\sigma}_i \otimes \hat{I} + u_{i+3}\hat{I} \otimes \hat{\sigma}_i + \sum_{j=1,2,3} u_{j+3(i+1)}\hat{\sigma}_i \otimes \hat{\sigma}_j)$, where $|\vec{u}| \leq \sqrt{3/8}$. For D-dimensional Hilbert space a density matrix contains $(D^2 - 1)$ independent parameters given as vector $\vec{u}$ and as many generalized Pauli operators [i.e., traceless generators of $SU(D)$], where $|\vec{u}| \leq \sqrt{(D-1)/2D}$. This fact makes the complete quantum state tomography a very challenging problem, as it requires an exponentially large number of measurements in relation to the number of qubits constituting the composite system (see, e.g., [26–28]). However, this otherwise problematic feature also opens a new possibility to encode $N = D^2 - 1$ parameters in a D-dimensional density matrix (i.e., the Hilbert-Schmidt space). Note, that for pure states the number of independent parameters is much lower, i.e., $N = 2D - 1$. In this way, by using mixed instead of pure states we can encode quadratically more features into a given state. Once the encoding is performed for M states a constant number of times, each distance can be measured in only three steps. This is because the HSD can be expressed by first-order overlaps $O(\hat{\rho}_i, \hat{\rho}_j)$ as described in Refs. [22,29,30]

$$D_{\mathrm{HS}}(\hat{\rho}_1, \hat{\rho}_2) = \sqrt{O(\hat{\rho}_1, \hat{\rho}_1) + O(\hat{\rho}_2, \hat{\rho}_2) - 2O(\hat{\rho}_1, \hat{\rho}_2)}, \qquad (2)$$

where the directly measured observables there are defined as $O(\hat{\rho}_i, \hat{\rho}_j) = \mathrm{Tr}(\hat{\rho}_i\hat{\rho}_j)$. If $\hat{\rho}_1 = \hat{\rho}_2$, we measure purity as discussed, e.g., in Refs. [31–33]. Each overlap or other functions of overlaps can be measured directly by utilizing multiparticle interactions between copies of the investigated states [22,29,32,34–39]. In contrast, by applying full quantum tomography (see, e.g., [26]) $(D^2 - 1)$ measurements are required to calculate the value of HSD. For technical reasons we measure each overlap by utilizing four positive-valued measures (POVMs). For $D = 4$ this amounts to 12 POVMs for obtaining a single value of D_{HS} in contrast to 32 measurements needed in the case of applying quantum state tomography (16 if two copies of a state are used in parallel). This discrepancy can become even greater in the case of larger values of D. The number of the required observables to measure in each of the three steps for a multiqubit overlap depends linearly on the number of qubits forming the density matrix, i.e., $n = \log_2(D)$ as $\mathcal{O}(n) = \mathcal{O}[\log_2(\sqrt{N+1})]$ (see, e.g., Refs. [29,35,37,39]). Thus, the complexity of the distance measurement is $\mathcal{O}(\log N)$.

Experimental setup.—Let us demonstrate the measurement of HSD in a linear-optical experiment with photons as information carriers. Here, the HSD is measured for two-qubit states by simultaneous interaction between four qubits. A straightforward approach uses four photons and only 1 degree of freedom (d.o.f.) such as polarization (see, e.g., Ref. [29]). Here we utilize 2 d.o.f. (polarization and spatial) to encode two qubits (see Fig. 2); therefore, only two photons were needed. In this way one achieves

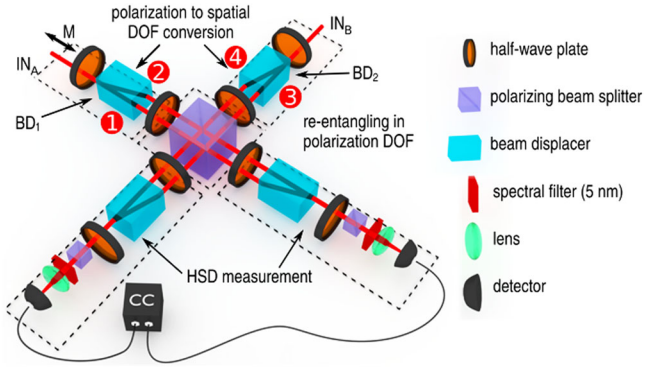

FIG. 3. Experimental setup for measuring the Hilbert-Schmidt distance of photonic two-qubit states. Spatial modes are labeled by numbers 1–4. IN_A and IN_B denote the input of photons A and B, respectively.

much higher detection rates which make the experiment considerably faster. The photons are labeled A and B, meanwhile their polarization and spatial modes are labeled p and s. There are horizontal (H) and vertical (V) polarization modes, and four spatial modes: 1–4 (see scheme in Fig. 3). We have associated a horizontally polarized photon with a logical state $|0\rangle$ and a vertically polarized photon with a logical state $|1\rangle$. Similarly, spatial modes 1 and 3 are associated with a logical state $|0\rangle$, modes 2 and 4 with a logical state $|1\rangle$. For example, photon A encodes state $|00\rangle$ if its polarization is made horizontal and it is placed in a spatial mode 1, i.e., in our notation $|H_1\rangle$.

The two photons are generated in a crystal cascade (known as the Kwiat source [40]) pumped by pulsed Paladine (coherent) laser at $\lambda = 355$ nm with 200 mW of mean optical power and a repetition rate of 120 MHz. The source consists of two BBO (β-BaB_2O_4) crystals and generates polarization-entangled photon pairs at λ=710nm, i.e., $|\Psi\rangle = \cos(\alpha)|HH\rangle + e^{i\theta}\sin(\alpha)|VV\rangle$. In this state, H and V stand for horizontal and vertical polarizations. The rates and mutual phase shift between horizontally and vertically polarized photons can be tuned by adjusting the pump beam polarization or by tilting one of the beam displacers (BD_1 or BD_2 in Fig. 3). By doing so one can prepare states with various amounts of entanglement. Each photon from the generated pair is coupled into a single-mode optical fiber and brought to one input port of the experimental setup depicted in Fig. 3. The photons then pass through beam displacers where the initial polarization encoding is transformed into spatial encoding. Afterwards the photons interact on the polarizing beam splitter (PBS) where a second, in principle different, quantum state is encoded into polarization d.o.f. As a result, two, in principle different, two-qubit states are encoded into the two d.o.f. The two states are then subjected to projective measurements as discussed below and accompanied by postselection. The photons are filtered by 5 nm interference filters, coupled into single-mode optical fibers and brought to single-photon detectors. Motorized translation M ensures temporal overlap of the photons on PBS. To demonstrate versatility of this approach, we have measured the HSD between four Bell states, four separable states, Werner states, and between Werner and Horodecki states.

To measure the HSD between any two states $(\hat{\rho}_1, \hat{\rho}_2)$ the first-order overlap has to be measured in three configurations, i.e., $O(\hat{\rho}_1, \hat{\rho}_1)$, $O(\hat{\rho}_2, \hat{\rho}_2)$, and $O(\hat{\rho}_1, \hat{\rho}_2)$. The first two configurations correspond to the situation when $\hat{\rho}_1$ ($\hat{\rho}_2$) is encoded into both d.o.f. During the last configuration $\hat{\rho}_1$ and $\hat{\rho}_2$ are encoded each in one d.o.f. Measurement of each first-order overlap $O(\hat{\rho}_1, \hat{\rho}_2)$ is split into a measurement of 4 POVMs on each photon across its d.o.f., i.e., $\hat{I}_A \otimes \hat{I}_B$, $\hat{S}_A \otimes \hat{I}_B$, $\hat{I}_A \otimes \hat{S}_B$, and $\hat{S}_A \otimes \hat{S}_B$, where the $\hat{I}$ stands for identity and the $\hat{S}$ for singlet state projection that were implemented by a suitable rotation of half-wave plates (HWPs) behind the PBS (for further information see the Supplemental Material [41]). For example, the POVM $\hat{I}_A \otimes \hat{I}_B$ consists of all combinations of local projections, i.e., $|H_1, H_3\rangle_{A,B}, |H_2, H_3\rangle_{A,B}, \ldots, |V_2, V_4\rangle_{A,B}$, while the $\hat{S}_A \otimes \hat{S}_B$ consists of projections $(1/\sqrt{2})(|H_2\rangle - |V_1\rangle)_A$ and $(1/\sqrt{2})(|H_4\rangle - |V_3\rangle)_B$. Both of these POVMs ($\hat{I}$, $\hat{S}$) can be implemented in a single step, but in this experiment they were implemented as a series of von Neumann projections. The coincidence rates corresponding to specific POVMs are labeled $f_{\hat{x}\hat{y}}$, where $\hat{x}, \hat{y} \in \{\hat{I}, \hat{S}\}$, where $\hat{x}$ and $\hat{y}$ are associated with photons A and B, respectively. These values are obtained by summing up the coincidence rates associated with respective von Neumann projections. The mean value of the overlap operators relates to these rates as

$$O(\rho_1, \rho_2) = 1 - 2(f_{\hat{S}\hat{I}} + f_{\hat{I}\hat{S}} - 2f_{\hat{S}\hat{S}})/f_{\hat{I}\hat{I}}. \qquad (3)$$

Note that POVMs associated with $f_{\hat{I}\hat{I}}$ measures the photon rate and is needed for normalization. In the case of a stable photon source and known setup parameters this value is constant and state independent. The same is true for POVMs $\hat{I}_A$ and $\hat{I}_B$ separately.

Experimental results.—First, we have measured the distances between four Bell states $|\Phi^{\pm}\rangle = (1/\sqrt{2})(|00\rangle \pm |11\rangle)$ and $|\Psi^{\pm}\rangle = (1/\sqrt{2})(|01\rangle \pm |10\rangle)$. Encoding of the states into the d.o.f. was implemented by a suitable choice of pump beam polarization, rotation of the HWPs, and by tilting one of the beam displacers (BD_1). We have decided to plot a second power of the HSD denoted D^2_{HS} so it is linear in terms of the physically measured quantities. The obtained experimental and theoretically calculated values of the second power of HSD between Bell states are shown in Fig. 4(a). Next, we have measured the HSD between separable states $|00\rangle$, $|11\rangle$, $|01\rangle$, and $|10\rangle$ and visualized the obtained values of D^2_{HS} in Fig. 4(b) (see also [41]).

In the third part of the experiment, we have calculated the values of D^2_{HS} between Werner states which up to a local

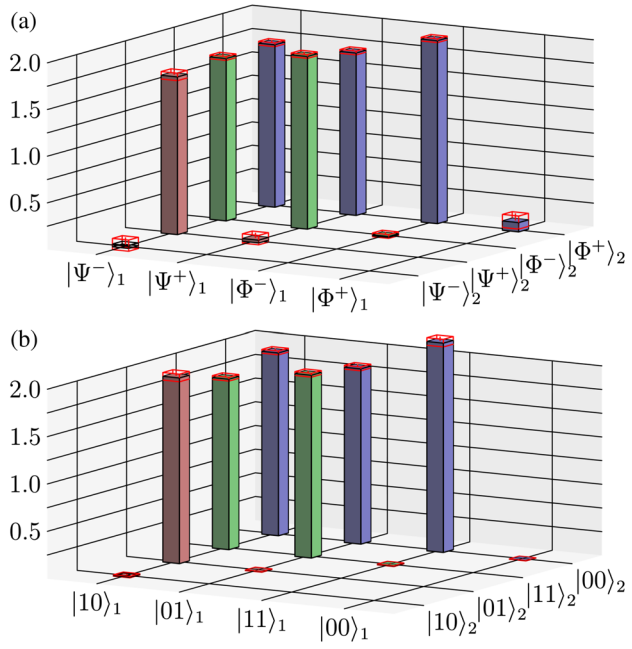

FIG. 4. Experimental results of the second power of the Hilbert-Schmidt distance D^2_{HS} between (a) Bell states, (b) separable states. The theoretical values are $D^2_{\mathrm{HS}} = 0$ for the diagonal elements and $D^2_{\mathrm{HS}} = 2$ for the off-diagonal elements. The indices represent spatial and polarization encoding, respectively (see Fig. 2).

unitary transformation can be expressed in a form of a weighted sum of maximally entangled and maximally mixed state

$$\hat{\rho}_W = p|\Phi^+\rangle\langle\Phi^+| + \frac{1}{4}(1-p)\hat{I}. \tag{4}$$

In the case of the mixed state, the outcome of each von Neumann projection was obtained by accumulating coincidence rates associated with four Bell states, i.e., making use of the identity $\hat{\rho}_1 \otimes \hat{\rho}_2 = \frac{1}{4}(|\Psi^+\rangle\langle\Psi^+| + |\Psi^-\rangle\langle\Psi^-| + |\Phi^+\rangle\langle\Phi^+| + |\Phi^-\rangle\langle\Phi^-|) = \frac{1}{4} I \otimes I$. Subsequently, we have calculated the D^2_{HS} between Werner states for various values of the weight parameter p. The results are visualized in Fig. 5(a). Finally, we have calculated the D^2_{HS} between Werner and Horodecki states. Horodecki states can be expressed in the form of a weighted sum of the maximally entangled and separable states

$$\hat{\rho}_H = q|\Phi^-\rangle\langle\Phi^-| + (1-q)|HV\rangle. \tag{5}$$

Therefore, we had to measure the overlap between states $|\Phi^+\rangle$ ($|\Phi^-\rangle$) and $|01\rangle$ encoded in polarization and spatial mode, respectively. The rest of the necessary overlaps were calculated in the same way as explained above. The values of D^2_{HS} between Werner and Horodecki states for various weight parameters p and q are visualized in Fig. 5(b).

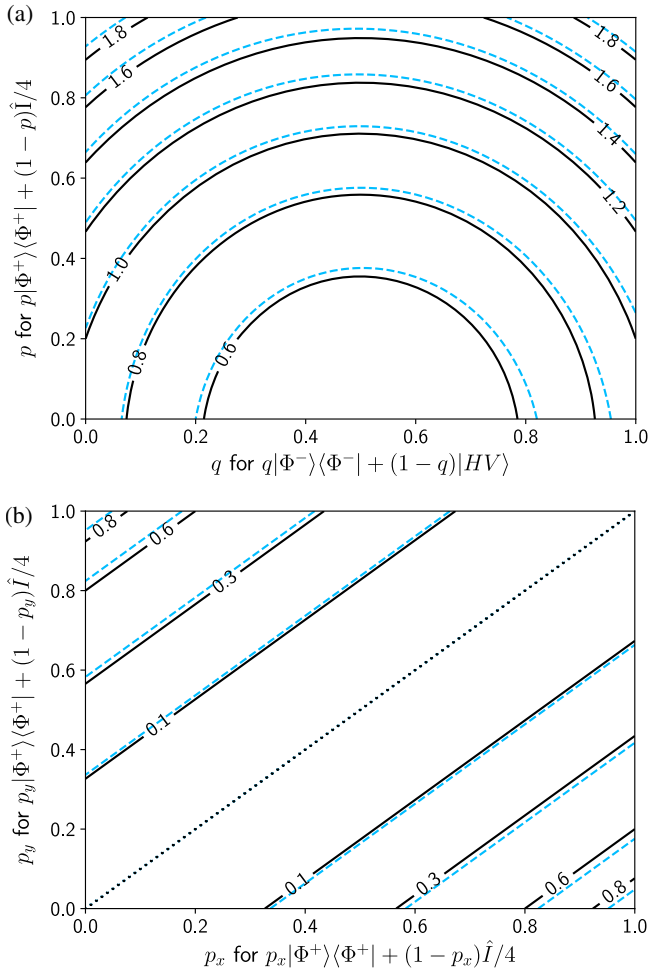

FIG. 5. Experimentally obtained values of D^2_{HS} (a) between two Werner states and (b) between Werner and Horodecki states for various weight parameters (p_x, p_y) or (p, q) are represented by corresponding light-shaded contours slightly shifted with respect to the labeled black contours representing the theoretical values of D^2_{HS}. The vertical and horizontal axes represent polarization and spatial encoding, respectively (see Fig. 2).

Conclusions.—We have reported on the experimental measurement of the Hilbert-Schmidt distance between two-qubit states by the method of many-particle interference. This method allows us to measure the HSD between two two-qubit density matrices by performing three overlap measurements (four POVMs per overlap) instead of 32 measurements required to directly all parameters of two two-qubit mixed states [28]. Our scheme works for both mixed and pure states; however, using the former is more desirable for machine learning. This is because for a system of a fixed dimension D we can encode quadratically more features in a mixed state than in a pure state. This approach to measuring Euclidean distance between a pair of points in space of dimension $N = D^2 - 1$ exhibits a reduced complexity of $\mathcal{O}(\log N)$ in comparison to the standard approach of the complexity $\mathcal{O}(\mathrm{poly}N)$. Optimizing the dependence

of the complexity on the number of data points M is out of the scope of this work. The obtained experimental results are in good agreement with theoretical predictions. To demonstrate the versatility of our approach we measured HSD between assorted two-qubit states. The HSDs between identical Bell states are sufficiently close to theoretical values. On the other hand, distances between orthogonal Bell states do not deviate from theoretical values by more than 15%. This error is partially caused by the linearization of Eq. (1) and by phase instability in the relatively complex interferometer. Further, partial distinguishability between photons causes an imperfect bunching that leads to partial impurities of the states, therefore, increasing the error. However, this discrepancy is implementation specific and not a fundamental limit. To assess the impact of measurement errors on the shape of two clusters created using a k-means algorithm with and without introducing a maximum error of 15% in distance measurement we performed numerical simulations. The initial sets of points were created using Gaussian distributions (see [41]). The clusters created for the range of distances between the Gaussians varying from 0 to 6 standard deviations differ on average by 4% of the points. We have obtained similar measurement results for the separable states; however, the deviation from the theoretical prediction is not as high due to the lower complexity of the states. We have also interpolated the HSDs between Werner states and between Werner and Horodecki states for various values of the weight parameters. The results are in good agreement with theoretical values represented by the contours in Fig. 5. We believe that these results can motivate subsequent research on the topic of quantum channel characterization and quantum machine learning. Especially in the latter, measuring distances between multidimensional points efficiently can reduce the computational complexity of supervised and unsupervised machine learning. Thus, our results can be inspiring for near term quantum technologies which would exhibit speedup in comparison to the best currently known classical solutions. Our results are also a novel example of applying mixed states for quantum information processing. Usually working with mixed states is not desired, but here it gives the possibility of encoding extra information as the degree of coherence between the given two dimensions of the density matrix.

The authors thank Cesnet for providing data management services. The authors acknowledge financial support by the Czech Science Foundation under Project No. 19-19002S. The authors also acknowledge Project No. CZ.02.1.01./0.0/0.0/16_019/0000754 of the Ministry of Education, Youth and Sports of the Czech Republic, and V. T. also acknowledges the Palacky University internal Grant No. IGA-PrF-2019-008.

*vojtech.travnicek@upol.cz
†karol.bartkiewicz@upol.cz
‡acernoch@fzu.cz
§k.lemr@upol.cz

[1] I. Marcikic, H. de Riedmatten, W. Tittel, H. Zbinden, M. Legré, and N. Gisin, Distribution of Time-Bin Entangled Qubits over 50 km of Optical Fiber, Phys. Rev. Lett. **93**, 180502 (2004).
[2] X.-S. Ma, T. Herbst, T. Scheidl, D. Wang, S. Kropatschek, W. Naylor, B. Wittmann, A. Mech, J. Kofler, E. Anisimova, V. Makarov, T. Jennewein, R. Ursin, and A. Zeilinger, Quantum teleportation over 143 kilometres using active feed-forward, Nature (London) **489**, 269 (2012).
[3] C. H. Benett and G. Brassard, Quantum Cryptography: Public key distribution and coin tossing, in *Proceedings of the IEEE International Conference on Computers, Systems, and Signal Processing, New York* (1984), Vol. 175, p. 175.
[4] A. K. Ekert, Quantum Cryptography Based on Bell's Theorem, Phys. Rev. Lett. **67**, 661 (1991).
[5] J. M. Renes, Equiangular spherical codes in quantum cryptography, Quantum Inf. Comput. **5**, 080 (2005).
[6] G. Alber, T. Beth, M. Horodecki, P. Horodecki, R. Horodecki, M. Rötteler, H. Weinfurter, R. Werner, and A. Zeilinger, *Quantum Information* (Springer, Berlin, 2001).
[7] D. Bowmeester, A. K. Ekert, and A. Zeilinger, *The Physics of Quantum Information* (Springer, Berlin, 2000).
[8] C. H. Benett, F. Bessette, G. Brassard, L. Salvail, and J. Smolin, Experimental quantum cryptography, J. Cryptol. **5**, 3 (1992).
[9] T. C. Ralph, Continuous variable quantum cryptography, Phys. Rev. A **61**, 010303(R) (1999).
[10] C. Croal, C. Peuntinger, B. Heim, I. Khan, C. Marquardt, G. Leuchs, P. Wallden, E. Andersson, and N. Korolkova, Free-Space Quantum Signatures Using Heterodyne Measurements, Phys. Rev. Lett. **117**, 100503 (2016).
[11] S. Pirandola, J. Eisert, C. Weedbrook, A. Furusawa, and S. Braunstein, Advances in quantum teleportation, Nat. Photonics **9**, 641 (2015).
[12] P. van Loock and S. L. Braunstein, Multipartite Entanglement for Continuous Variables: A Quantum Teleportation Network, Phys. Rev. Lett. **84**, 3482 (2000).
[13] D. Castelvecchi, The quantum internet has arrived (and it hasn't), Nature (London) **554**, 289 (2018).
[14] A. Barasiński, I. I. Arkhipov, and J. Svozilík, Localizable entanglement as a necessary resource of controlled quantum teleportation, Sci. Rep. **8**, 15209 (2018).
[15] H. Yonezawa, T. Aoki, and A. Furusawa, Demonstration of a quantum teleportation network for continuous variables, Nature (London) **431**, 430 (2004).
[16] A. Barasinski, A. Černoch, and K. Lemr, Demonstration of Controlled Quantum Teleportation for Discrete Variables on Linear Optical Devices, Phys. Rev. Lett. **122**, 170501 (2019).
[17] W. K. Zurek and W. H. Wooters, A single quantum cannot be cloned, Nature (London) **299**, 66 (1982).
[18] K. Bartkiewicz, K. Lemr, A. Černoch, J. Soubusta, and A. Miranowicz, Experimental Eavesdropping Based on Optimal Quantum Cloning, Phys. Rev. Lett. **110**, 173601 (2013).

[19] K. Bartkiewicz, A. Černoch, G. Chimczak, K. Lemr, A. Miranowicz, and F. Nori, Experimental quantum forgery of quantum optical money, npj Quantum Inf. **3**, 7 (2017).
[20] I. Bengtsson and K. Życzkowski, *Geometry of Quantum States: An Introduction to Quantum Entanglement* (Cambridge University Press, Cambridge, England, 2017).
[21] J. Dajka, J. Łuczka, and P. Hänggi, Distance between quantum states in the presence of initial qubit-environment correlations: A comparative study, Phys. Rev. A **84**, 032120 (2011).
[22] K. Bartkiewicz, V. Trávníček, and K. Lemr, Measuring distances in Hilbert space by many-particle interference, Phys. Rev. A **99**, 032336 (2019).
[23] X.-D. Cai, D. Wu, Z.-E. Su, M.-C. Chen, X.-L. Wang, L. Li, N.-L. Liu, C.-Y. Lu, and J.-W. Pan, Entanglement-Based Machine Learning on a Quantum Computer, Phys. Rev. Lett. **114**, 110504 (2015).
[24] S. Lloyd, M. Mohseni, and P. Rebentrost, Quantum algorithms for supervised and unsupervised machine learning, arXiv:1307.0411.
[25] J. Biamonte, P. Wittek, N. Pancotti, P. Rebentrost, N. Wiebe, and S. Lloyd, Quantum machine learning, Nature (London) **549**, 195 (2017).
[26] *Quantum State Estimation*, edited by M. Paris and J. Řeháček (Springer, Berlin, 2004).
[27] A. Miranowicz, K. Bartkiewicz, J. Peřina, M. Koashi, N. Imoto, and F. Nori, Optimal two-qubit tomography based on local and global measurements: Maximal robustness against errors as described by condition numbers, Phys. Rev. A **90**, 062123 (2014).
[28] K. Bartkiewicz, A. Černoch, K. Lemr, and A. Miranowicz, Priority choice experimental two-qubit tomography: Measuring one by one all elements of density matrices, Sci. Rep. **6**, 19610 (2016).
[29] C. Zhang, B. Yadin, Z.-B. Hou, H. Cao, B.-H. Liu, Y.-F. Huang, R. Maity, V. Vedral, C.-F. Li, G.-C. Guo, and D. Girolami, Detecting metrologically useful asymmetry and entanglement by a few local measurements, Phys. Rev. A **96**, 042327 (2017).
[30] R. Filip, Overlap and entanglement-witness measurements, Phys. Rev. A **65**, 062320 (2002).
[31] F. A. Bovino, G. Castagnoli, A. Ekert, P. Horodecki, C. M. Alves, and A. V. Sergienko, Direct Measurement of Nonlinear Properties of Bipartite Quantum States, Phys. Rev. Lett. **95**, 240407 (2005).
[32] K. Bartkiewicz, K. Lemr, and A. Miranowicz, Direct method for measuring of purity, superfidelity, and subfidelity of photonic two-qubit mixed states, Phys. Rev. A **88**, 052104 (2013).
[33] K. Lemr, K. Bartkiewicz, and A. Černoch, Experimental measurement of collective nonlinear entanglement witness for two qubits, Phys. Rev. A **94**, 052334 (2016).
[34] A. K. Ekert, C. M. Alves, D. K. L. Oi, M. Horodecki, P. Horodecki, and L. C. Kwek, Direct Estimations of Linear and Nonlinear Functionals of a Quantum State, Phys. Rev. Lett. **88**, 217901 (2002).
[35] C. M. Alves and D. Jaksch, Multipartite Entanglement Detection in Bosons, Phys. Rev. Lett. **93**, 110501 (2004).
[36] T. A. Brun, Measuring polynomial functions of states, Quantum Inf. Comput. **4**, 401 (2004).
[37] H. Jeong, C. Noh, S. Bae, D. G. Angelakis, and T. C. Ralph, Detecting the degree of macroscopic quantumness using an overlap measurement, J. Opt. Soc. Am. B **31**, 3057 (2014).
[38] K. Bartkiewicz, K. Lemr, A. Černoch, and A. Miranowicz, Bell nonlocality and fully entangled fraction measured in an entanglement-swapping device without quantum state tomography, Phys. Rev. A **95**, 030102(R) (2017).
[39] R. Islam, R. Ma, P. M. Preiss, M. E. Tai, A. Lukin, M. Rispoli, and M. Greiner, Measuring entanglement entropy in a quantum many-body system, Nature (London) **528**, 77 (2015).
[40] P. G. Kwiat, E. Waks, A. G. White, I. Appelbaum, and P. H. Eberhard, Ultrabright source of polarization-entangled photons, Phys. Rev. A **60**, R773 (1999).
[41] See Supplemental Material at http://link.aps.org/supplemental/10.1103/PhysRevLett.123.260501 for more details on the theoretical framework, experimental implementation and obtained results.